Proceedings of the Fortieth Turbomachinery Symposium
September 12-15, 2011, Houston, Texas

TILTING-PAD BEARINGS: MEASURED FREQUENCY CHARACTERISTICS OF THEIR ROTORDYNAMIC COEFFICIENTS

Dara W. Childs
Leland T. Jordan Professor
Turbomachinery Laboratory
Texas A&M University
College Station, TX, USA

Adolfo Delgado
Mechanical Engineer
Global Research Center
General Electric
Niskayuna, NY, USA

Giuseppe Vannini
Senior Engineer
Conceptual Advanced Mechanical Design
GE Oil & Gas
Florence, Italy

ABSTRACT

This paper reviews a long standing issue related to the stiffness and damping coefficients of tilting-pad (TP) bearings; namely, *What is the nature of their frequency dependency?* A research project was implemented at the Turbomachinery Laboratory (TL) at Texas A&M University (TAMU) around 2003 to examine the issue, applying procedures that had been developed and used to investigate the rotordynamic characteristics of annular gas seals. Those seals, using a smooth rotor and a honeycomb or hole-pattern stator were predicted to have strongly frequency-dependent reaction forces that could not be modeled by a combination of stiffness, damping, and inertia coefficients. Measurements confirmed the strongly frequency dependent nature of their stiffness and damping coefficients.

Subsequent test have examined the following bearing types: (i) Two-axial-groove bearing, (ii) pressure dam bearings, (iii) Flexure-pivot-pad tilting-pad bearing (FPTP) in load-on-pad (LOP) and load-between-pad (LBP), (iv) Rocker-pivot-pad TP bearing in LOP and LBP configurations at two different preloads and 50 and 60% offsets, and (v) a spherical seat bearing in LOP and LBP configurations. Representative test results are presented for some of these bearings. In addition, this paper includes experimental results for 5-pad and 4-pad tilting pad bearings (with similar features to TAMU configuration iv) tested at the GE Global Research Facility (GRC) as part of an independent research initiative from GE Oil and Gas.

Frequency effects on the dynamic-stiffness coefficients were investigated by applying dynamic-force excitation over a range of excitation frequencies. Generally, *for all bearings tested* at TAMU and GRC, the direct real parts of the dynamic-stiffness coefficients could be modeled as quadratic functions of the excitation frequency and accounted for by adding a mass matrix to the conventional [*C*][*K*] model to produce a frequency-independent [*M*][*C*][*K*] model. Additionally, the direct damping could be modeled by a constant, frequency-independent coefficient. Consequently, these experimental findings from two independent sources support the use of synchronously reduced force coefficients for characterizing the dynamic performance of tilting pad bearings in Oil and Gas applications, as prescribed by API 617 7th edition (Process Centrifugal Compressors) and more generally by API684 Rotordynamic Tutorial.

INTRODUCTION

In 1964, Lund calculated the stiffness and damping coefficients for a single, fixed, nonrotational pad and then summed the contributions from each pad to find the combined effect of the pad assembly. This procedure is "Lund's Pad Assembly Method." Lund's design curves do not account for frequency dependency. For many years, the common assumption was that the coefficients should be calculated at the synchronous frequency. Several authors have produced calculated results for tilting pad bearings showing a significant frequency dependency for the coefficients in a [C][K] model; Warner and Soler raised the issue in 1975.

Figure 1 shows a spring in series with a fluid-film model that produces frequency-dependent stiffness and damping coefficients.

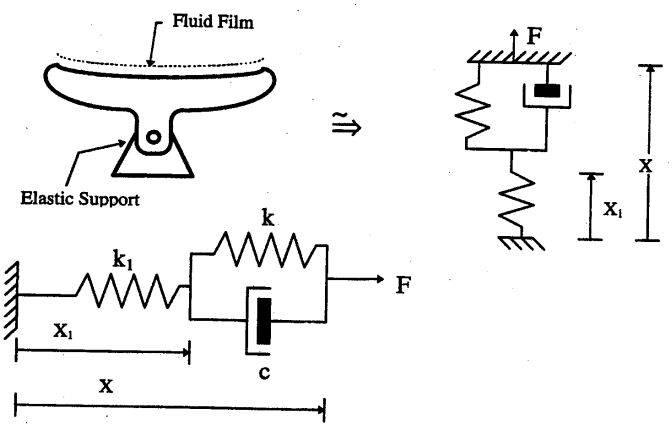

Figure 1. Flexible support of a parallel spring-damper assembly (Childs, 2002)

Eliminating the X_1 coordinate gives the frequency-domain model

$$F(j\Omega)/X(j\Omega) = -[(k+jc\Omega)k_1]/[(k+k_1)+jc\Omega]$$
$$= -\frac{[kk_1((k+k_1)+k_1c^2\Omega^2]+jck_1^2\Omega]}{(k+k_1)^2+c^2\Omega^2}$$
$$= -[\frac{kk_1}{k+k_1}+\frac{c^2\Omega^2k_1^2}{(k+k_1)^3}+...]-jc\Omega[\frac{k_1^2}{(k+k_1)^2}-\frac{c^2\Omega^2k_1^2}{(k+k_1)^4}+...]$$
$$= -[K(\Omega)_{eff}+jC(\Omega)_{eff}\Omega] \quad (1)$$

At low frequencies, Eq.(1) predicts that the fluid-film stiffness k is reduced by the factor $k_1/(k + k_1)$, and the damping c is reduced by $[k_1/(k + k_1)]^2$. At higher frequencies, K_{eff} and C_{eff} increase and decrease, respectively, with increasing frequency.

A test program was launched at the Turbomachinery Laboratory (TL) at Texas A&M University (TAMU) to investigate the frequency dependent behavior of tilting-pad bearings, and this paper summarizes results from that program plus results from other test programs.

TEST RIG AND IDENTIFICATION TECHNIQUES

Figure 2 provides a side view of the test rig. It copies Glenicke's "shake the stator" idea. The test bearing is placed at the center of a rotor that is supported on both ends by mist-lubricated hybrid ceramic ball bearings. The test bearing is supported in a housing that is attached to the support-bearing pedestals via "pitch stabilizers." The pitch stabilizers consist of two pairs of three opposed turnbuckles that are spaced at 120 degree arcs around the housing. They allow the bearing housing to move freely in the radial direction yet prevent pitch and yaw rotations and axial movement. Power is delivered to the rotor from a 65 KW (90HP) air turbine through a flexible coupling. Speed can be varied up to 16k rpm.

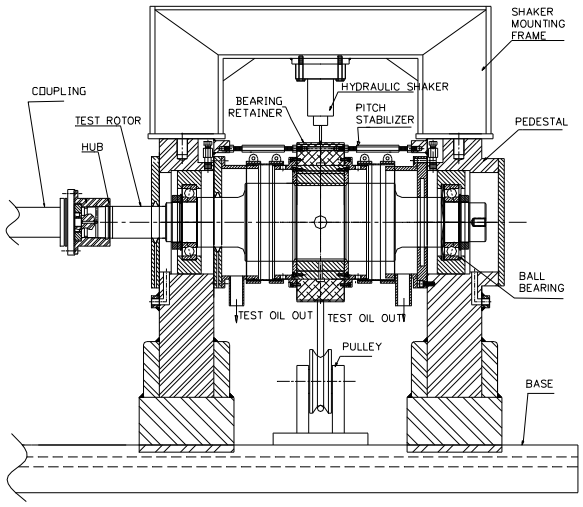

Figure.2 Cross sectional view of test stand (Al-Ghasem and Childs)

A pneumatic loader is used to apply a steady tensile load up to 22 kN in the *y* direction of figure 3. The hydraulic shaker connections shown in Fig. 3 deliver dynamic forces to the bearing housing that are parallel and perpendicular to the static load. Forces are transmitted from hydraulic shakers to the bearing housing through stingers. Load cells in the shaker heads measure the dynamic forces.

A pseudo-random waveform that includes all frequencies from 20-320 Hz in 20Hz intervals is the input signal to the hydraulic shakers. The amplitude and phase of the wave-form components are determined to minimize the peak force required from the shaker while providing adequate response amplitudes within the bearing, Stanway et al.

As shown in Fig. 3, two piezoelectric accelerometers are attached to the bearing housing. Eddy-current proximity probes measure rotor-bearing relative-displacement components in the *x* and *y* bearing-housing axes. Two probes are located in plane at the drive end; two are located in a parallel plane at the non-drive end. Because measurements are taken in two parallel planes, both the pitch and yaw of the stator housing (relative to the rotor axis) can be measured and minimized prior to testing.

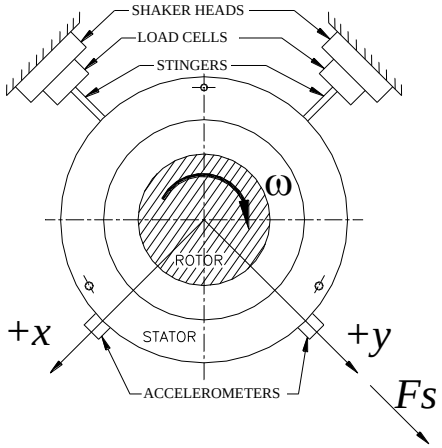

Figure. 3 Test bearing stator attached to shakers via stingers; static load F_s in +y direction (Al-Ghasem and Childs)

Dynamic-Stiffness-Coefficient Identification

The dynamic data sets are used to determine the rotordynamic stiffness, damping, and added-mass coefficients, using a process described by Rouvas and Childs. Applying Newton's second law to the stator gives

$$M_s\begin{bmatrix}\ddot{x}_s\\ \ddot{y}_s\end{bmatrix}=\begin{bmatrix}f_x\\ f_y\end{bmatrix}-\begin{bmatrix}f_{bx}\\ f_{by}\end{bmatrix} \quad (2)$$

For this equation, the housing assembly is assumed to be a rigid body, and the test results obtained are consistent with that assumption. In Eq.(2), M_s is the stator mass, $\ddot{x}_s, \ddot{y}_s$ are the stator accelerations components, f_x, f_y are the force components produced by the hydraulic shakers, and f_{bx}, f_{by} are the

reaction-force components. Assuming that the bearing reaction forces are modeled by the following [*M*][*C*][*K*] model,

$$-\begin{bmatrix} f_{bx} \\ f_{by} \end{bmatrix} = \begin{bmatrix} K_{xx} & K_{xy} \\ K_{yx} & K_{yy} \end{bmatrix} \begin{bmatrix} \Delta x \\ \Delta y \end{bmatrix} + \begin{bmatrix} C_{xx} & C_{xy} \\ C_{yx} & C_{yy} \end{bmatrix} \begin{bmatrix} \Delta \dot{x} \\ \Delta \dot{y} \end{bmatrix} + \\ + \begin{bmatrix} M_{xx} & M_{xy} \\ M_{yx} & M_{yy} \end{bmatrix} \begin{bmatrix} \Delta \ddot{x} \\ \Delta \ddot{y} \end{bmatrix} \quad (3)$$

The relative bearing-stator displacements in this equation are measured by eddy-current displacement probes. Substituting from Eq.(3) into Eq.(2) and applying an FFT produces:

$$\begin{bmatrix} \boldsymbol{F}_x - M_s \boldsymbol{A}_x \\ \boldsymbol{F}_y - M_s \boldsymbol{A}_y \end{bmatrix} = -\begin{bmatrix} \boldsymbol{H}_{xx} & \boldsymbol{H}_{xy} \\ \boldsymbol{H}_{yx} & \boldsymbol{H}_{yy} \end{bmatrix} \begin{bmatrix} \boldsymbol{D}_x \\ \boldsymbol{D}_y \end{bmatrix} \quad (4)$$

These two equations have the four dynamic-stiffness functions H_{ij} as unknowns. Shaking alternately in the *x* and *y* directions provides four independent equations. The dynamic-stiffness functions H_{ij} are related to the rotordynamic coefficients via:

$$\boldsymbol{H}_{ij} = K_{ij} - \Omega^2 M_{ij} + j(\Omega C_{ij}) \quad (5)$$

Hence,

$$\mathrm{Re}(\boldsymbol{H}_{ij}) = K_{ij} - \Omega^2 M_{ij} \quad (6)$$

$$\mathrm{Im}(\boldsymbol{H}_{ij}) = \Omega C_{ij} \quad (7)$$

Nothing about the test or identification procedures force the dynamic stiffness coefficients to have the form of Eq.(5). Identical test and identification procedures were used for gas annular seals with smooth rotors and either honeycomb (Sprowl and Childs) or hole-pattern (Childs and Wade) stators for which the stiffness and damping coefficients are strongly frequency dependent. Figure 4 illustrates measured and predicted rotordynamic coefficients for an annular gas seal. The direct stiffness coefficient on the left is increasing with excitation frequency. The direct damping coefficient on the right is falling with increasing excitation frequency. Measured direct and cross-coupled stiffness and damping coefficients were also strongly frequency dependent.

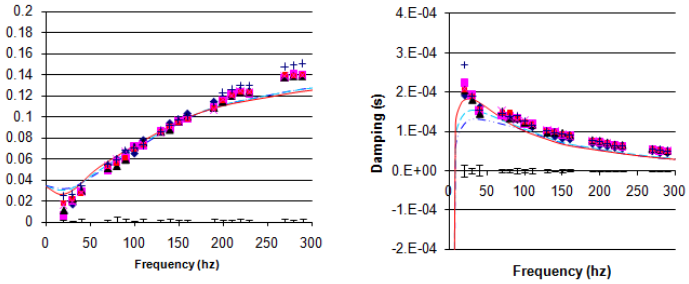

Figure. 4 Measured, nondimensionalized direct stiffness (left) and normalized direct damping (right) for an annular honeycomb-stator seal (*Weatherwax and Childs*)

Test Bearings

Tests have been conducted for the following configurations:

1. Cylindrical with two axial grooves (Al-Jughaiman)
2. Pressure-dam **(**Al-Jughaiman and Childs)
3. Flexure pivot-pad in LOP (Rodriguez and Childs**)** and LBP configurations (Al-Ghasem and Childs)
4. 5-pad, rocker-pivot-pad bearing in LOP (Carter and Childs) and LBP (Childs and Carter) configurations. This configuration has been tested for two preloads at 60% and one preload at 50% offsets.
5. A spherical-seat bearing (Harris and Childs)

Details of the bearing geometries and test conditions can be found in the cited references and are not repeated here. The nature of the measured results in regard to the frequency-dependent behavior is of interest.

Experimental Procedure

The coefficients of Eqs. (6-7) are estimated from a set of dynamic-stiffness data that can introduce sampling and curve-fitting errors. Uncertainty terms are accordingly required to indicate the estimate accuracy. The uncertainty is found by using a 95% confidence interval that measures the error bound for the estimate of the slope or intercept.

A baseline test is performed to find the dynamic coefficients of the test-rig structure alone. To get the base-line contribution, a "dry shake" test is performed at zero speed with no lubricant. The $\boldsymbol{H}_{ij}$ dry-shake test results are subtracted from the measured bearing test results.

Measured Results for a 2-axial groove bearing

Figure 5 illustrates measured values for *Re* ($\boldsymbol{H}_{xx}$) and *Re* ($\boldsymbol{H}_{yy}$) for the 2-axial groove bearing. These results are easily fitted with a quadratic to produce *constant* direct stiffness (K_{xx}, *Kyy*) and apparent mass ($M_{xx,}$ M_{yy}) coefficients. . In fact, the measured values for M_{XX}, M_{YY} agree reasonably well with the predictions of Reinhardt and Lund. Figure 6 illustrates a companion plot of *Re* ($\boldsymbol{H}_{XY}$) and *Re* ($\boldsymbol{H}_{YX}$). The curves are frequency independent and produce constant cross-coupled stiffness coefficients, K_{YX}, K_{XY}.

Figure 7 illustrates *Im* **(**$\boldsymbol{H}_{XX}$**)**, *Im* **(**$\boldsymbol{H}_{XY}$**)**, *Im* **(**$\boldsymbol{H}_{YX}$**)**, and *Im* **(**$\boldsymbol{H}_{YY}$**)** versus Ω. These functions are readily fit by straight lines producing constant damping coefficients C_{XX}, C_{YY}, C_{YX}, *and CXY*. Al-Jughaiman reported generally good agreement between measurements and predictions for this bearing using either a Reynolds-equation or a bulk-flow Navier-Stokes model.

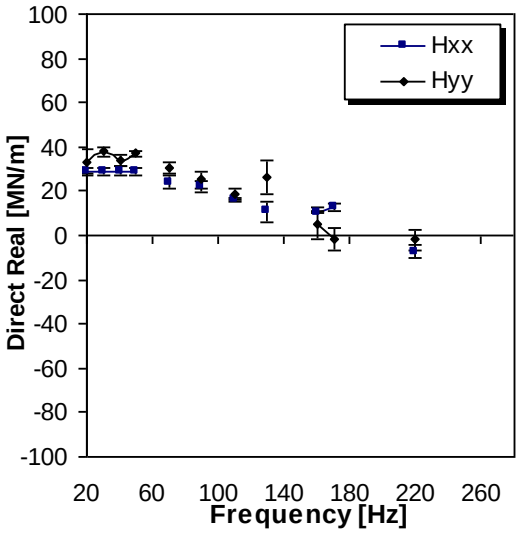

Figure. 5 Re (H_{XX}) and Re (H_{YY}) versus Ω for a 2-axial groove bearing (*Al-Jughaiman*)

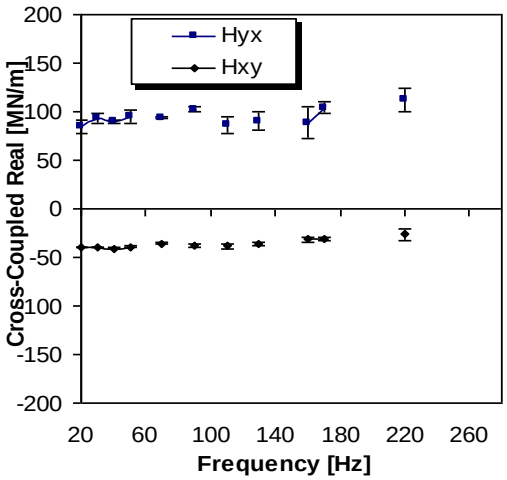

Figure. 6 Re (H_{YX}) and Re (H_{XY}) versus Ω for a 2-axial groove bearing (*Al-Jughaiman*)

So far, the results show: (i) The test procedures and identification procedures used can identify frequency-dependent stiffness and damping coefficients, and (ii) Measured results for a 2-axial groove bearing are as expected and in reasonable agreement with expectations. The outcomes for the pressure-dam bearing basically parallel those for the 2-axial-groove bearing.

Figure 8 illustrates a flexure-pivot-pad tilting-pad bearing. The pads can tilt, but are restrained by the elastic steel column that supports them. The bearings tested by Al-Ghasem and Childs, and Rodriguez and Childs were as illustrated in figure 8, 4-pads with 50% offset. The results were similar to those for the fixed-arc bearings in terms of frequency dependency; however, high uncertainty values for $Im(\boldsymbol{H_{XY}})$, $Im(\boldsymbol{H_{YX}})$, prevented identification of C_{XY} , C_{YX} . Reasonable agreement was found between measurement and theory using either a Reynolds equation model or a bulk-flow model in Rodriguez and Childs and Al-Ghasem and Childs.

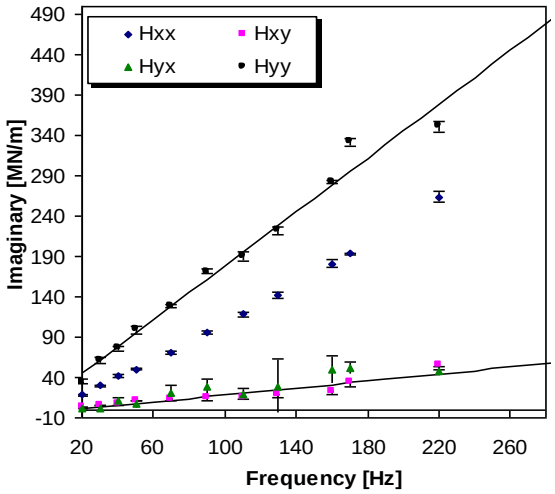

Figure. 7 Im (H_{XX}) , Im(H_{XY}), Im(H_{YX}), and Im(H_{YY}) versus Ω for a 2-axial groove bearing (*Al-Jughaiman*)

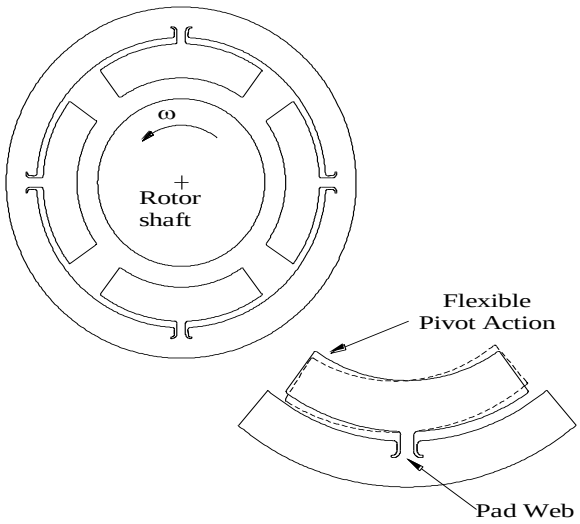

Figure. 8 Flexure-pivot-pad bearing (*Rodriguez and Childs)*

Rocker-pivot-pad bearing results

Figure 9 provides views from the end and side of a five-pad, rocker-pivot TP bearing. Lubrication is applied directly to a pad via the leading edge groove (LEG) shown in Fig. 10. The leading edge is called a "flow director." It wipes and redirects hot carryover oil away from the cool oil that is being injected into the leading edge recess. This design was pioneered by Ball and Byrne. Table 1 provides details of the bearing geometry.

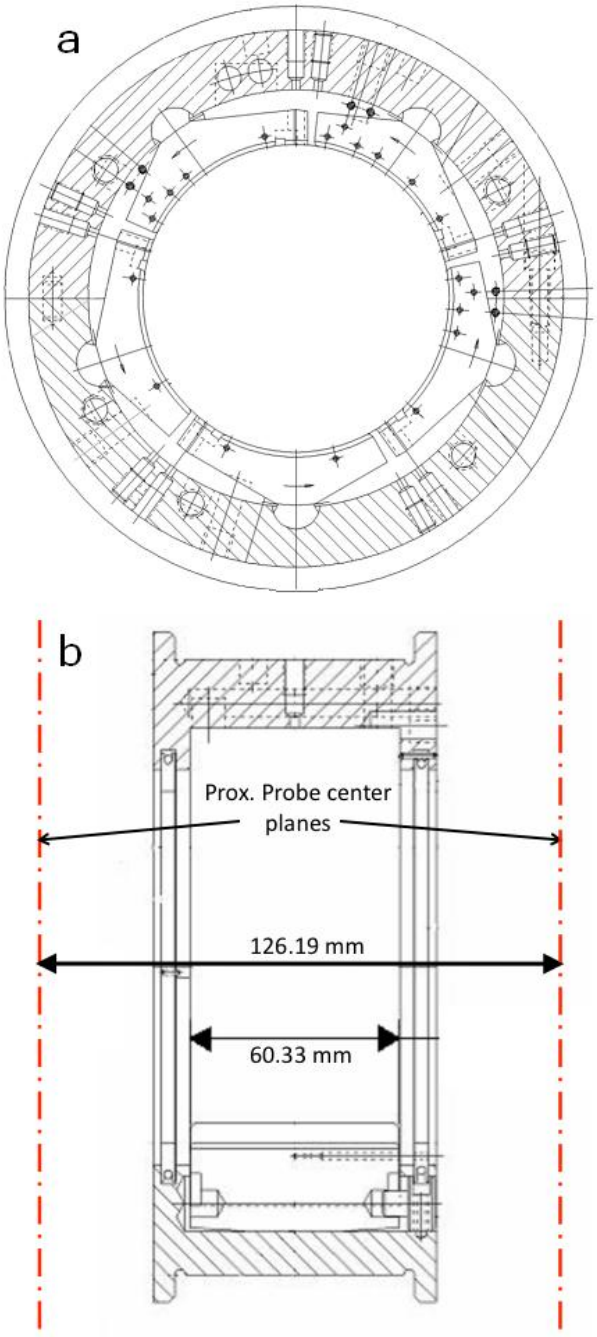

Figure. 9 5-pad, rocker-pad bearing in LOP configuration; (a) End view, (b) Side view showing measurement planes

Measured $\boldsymbol{H}_{ij}$ coefficients associated with 13 krpm and 345 kPa are shown in Fig. 11. The 60% offset results are taken from Carter and Childs. The 50% offset results are taken from current research. The "bars" in the data reflect the repeatability uncertainties from 32 repeated tests at the same operating condition. For a 60% offset, Figure 11a shows Re($\boldsymbol{H}_{yy}$) to be substantially larger than Re($\boldsymbol{H}_{xx}$) at low frequencies with the two functions approaching the same magnitude around $\Omega=\omega$. The 60% offset results are similar, although the projected stiffness values (at zero frequencies) are smaller and the curvature values are also smaller projecting to smaller apparent-mass coefficients. The measured results are readily fitted with the quadratic function of Eq.(6).

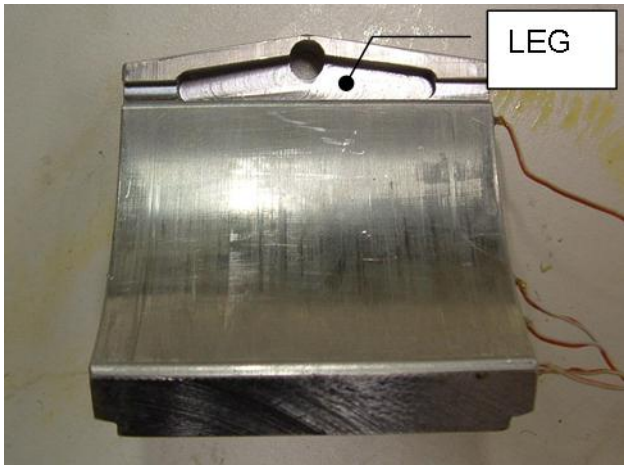

Figure 10 Leading-edge groove TP bearing pad

Table 1 Test rocker-pivot-pad TP bearing Specifications

Number of pads	5
Configuration	LBP and LOP
Pad arc angle	57.87˚
Pivot offset	60%, 50%
Rotor Diameter	101.587 mm (3.9995 in)
Pad axial length	60.325 mm (2.375 in)
Diametrical pad clearance	.221 mm (.0087 in)
Diametrical bearing clearance	.1575 mm (.0062 in)
Preload	.282
Radial pad clearance (C_p)	.1105 mm (.00435 in)
Radial bearing clearance (C_b)	.0792 mm (.00312 in)
Pad polar inertia	0.000249 kgm^2
Pad mass	.44 kg (.96 lb)
Lubricant type	ISO VG32

Figure 11b illustrates Re($\boldsymbol{H}_{yx}$) and Re($\boldsymbol{H}_{xy}$), showing little differences between the 50% and 60% results. These functions are also readily fitted with the quadratic function of Eq.(6). Near zero values are predicted for these functions. Re($\boldsymbol{H}_{yx}$) and Re($\boldsymbol{H}_{xy}$), have about the same positive curvature, predicting negative and approximately equal m_{xy} and m_{yx} coefficients. Note, that they do not impact stability.

Figure 11c shows Im($\boldsymbol{H}_{xx}$), Im($\boldsymbol{H}_{yy}$) versus Ω with Im($\boldsymbol{H}_{yy}$)>Im($\boldsymbol{H}_{xx}$) implying $C_{yy}>C_{xx}$ for both 50% and 60% offset ratios. The measurements predict a near zero intercept for both functions at $\Omega=0$. Both results are readily fit with the linear function of Eq.(7). The author has frequently spoken with analysts (and anonymous reviewers) who believe that a 50% offset tilting pad bearing will have frequency-dependent direct damping coefficients; however, these results show constant, frequency-dependent damping coefficients. Schmied

et al. present predictions of frequency dependency in the 2010 IFToMM conference for 55% offset tilting-pad bearings.

Measured results are not presented for Im($\boldsymbol{H}_{xy}$) and Im($\boldsymbol{H}_{yx}$). For rocker-pivot-pad tilting-pad bearings, they tend to be erratic functions of Ω with high uncertainties

Predictions for these bearings were reasonable for the load-deflection measurements and direct stiffness coefficients but poor for the direct damping coefficients, with comparable predictions using either a Reynolds equation model or a bulk-flow model. Measured direct damping coefficients were insensitive to chances in load conditions, versus predictions of strong sensitivity at low loads.

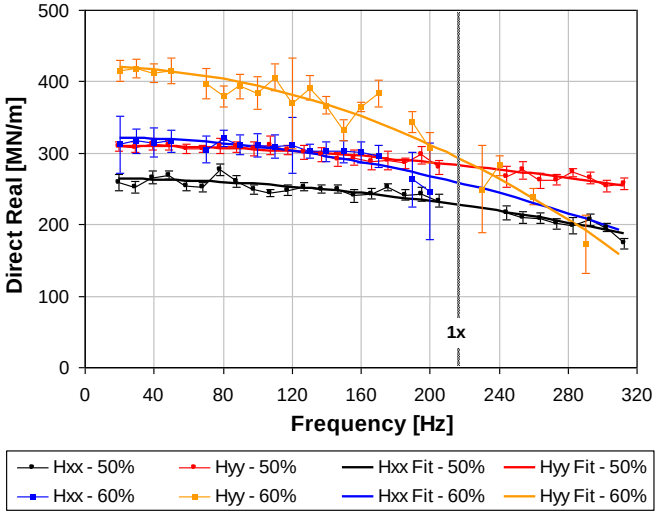

Figure. 11a LBP Real direct dynamic stiffness coefficients at 13 krpm and 345 kPa for: 50% and 60% offsets

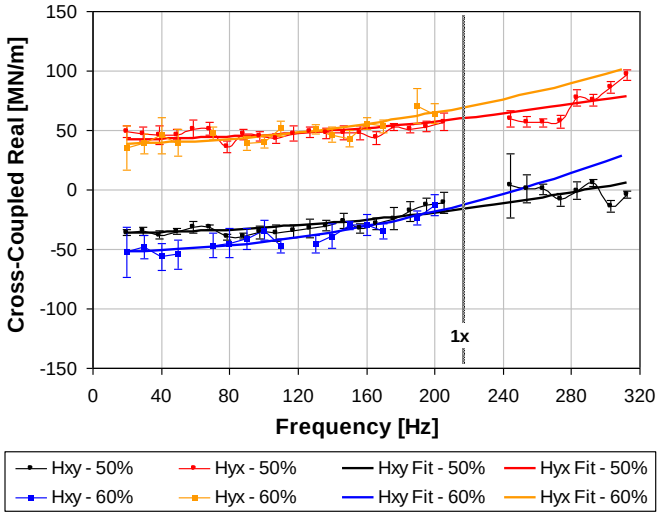

Figure 11b LBP Imaginary quadrature dynamic stiffness coefficients at 13 krpm and 345 kPa for: 50% and 60% offsets

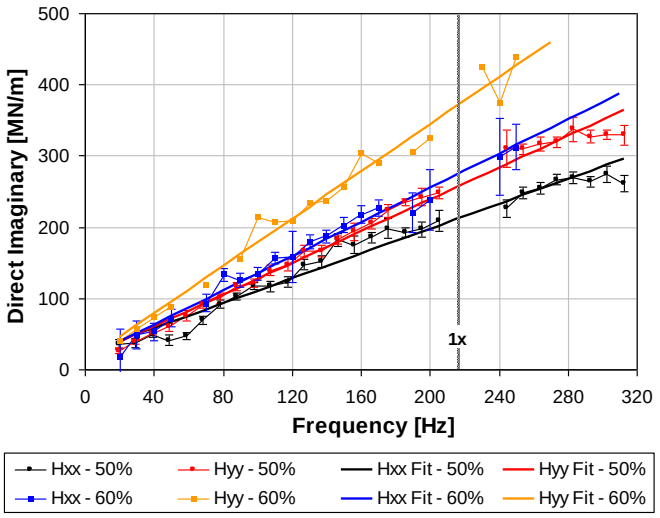

Figure. 11c Imaginary direct dynamic stiffness coefficients at 13 krpm and 345 kPa for: 50% and 60% offsets

As noted above, Harris and Childs tested a spherical-seat tilting-pad bearing, and Table 2 summarizes its properties. The results regarding frequency dependency were similar to those for the rocker-pivot pad bearings, except for a significantly more flexible backup structure. Figure 12 illustrates *Im*($\boldsymbol{H}_{xx}$), *Im*($\boldsymbol{H}_{yy}$) versus Ω for this bearing, and some frequency dependency is evident. This observed dependency consists of a small drop in slope with increasing frequency, particularly at higher excitation frequencies.

The result indicates a drop in damping with increasing frequency and is consistent with Eq.(1) but at odds with the commonly held view that damping is lower at the rotor's natural frequency than at running speed.

Table 2. Test spherical-seat TP bearing parameters (*Harris and Childs*).

Number of pads	4
Configuration	LBP
Pad arc angle	73°
Pivot offset	65%
Rotor diameter	101.59 ± 0.01 mm (3.9995 ± 0.0005 in)
Pad axial length	101.60 ± 0.03 mm (4.000 ± 0.001 in)
Manufacturer-reported radial bearing clearance (C_b)	95.3 μm (3.75 mils)
Mean Loaded Pad Preload	0.37
Mean Unloaded Pad Preload	0.58
Ball Radius of Curvature (Design)	3.175 + 0.0008 - 0 cm (1.25 + 0.0003 - 0 in)
Ball Material	4140 Rc 52 Steel w/ 12L14 Steel Support Shim
Socket Radius of Curvature (Design)	3.175 ± 0.013 cm (1.25 + 0.005 in)
Socket Material	Bronze
Lubricant Type	ISO VG32

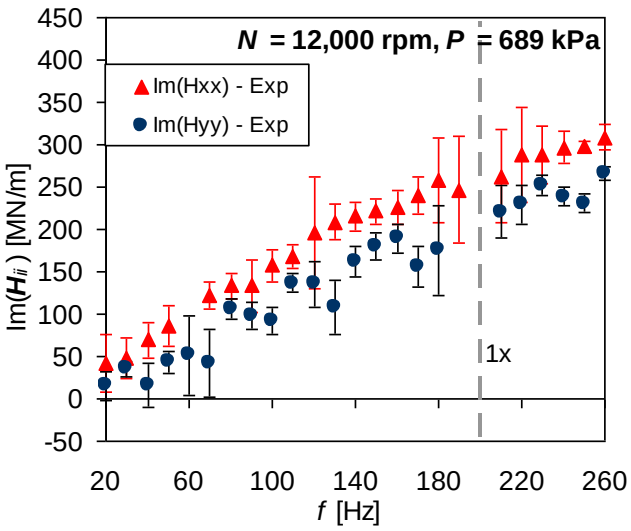

Figure 12. Im(H_{xx}), Im(H_{yy}) at 12,000 rpm for a spherical-seat bearing, 689 kPa (100 psi) (Harris and Childs).

FORCE COEFFICIENTS FOR A 5-PAD AND 4-PAD TILTING PAD BEARING TESTED IN AN INDEPENDENT EXPERIMENTAL FACILITY

Force coefficients for 5-pad and 4-pad bearing configurations were identified at General Electric Research Center (GE-GRC) as part of an independent test initiative from GE Oil and Gas (GE-O&G) to characterize the dynamic response of tilting pad bearings and investigate the frequency dependence of the resulting force coefficients. This section describes the test facility, test bearing and presents the experimentally identified force coefficients. Most of the results and findings in this section were presented by Delgado et. al. in 2010.

Test rig and Bearing Description

Similar to the TAMU-TL test facility, the design of the bearing test rig is based on Glenicke's concept, in which the test bearing is mounted on a flexible structure and the forces are applied onto the bearing externally through the housing. Figure 13 depicts a front and cut view of the test rig. The precision balanced test rotor is supported on two pairs of back-to-back precision angular contact bearings (slave bearings). The slave bearings are lubricated with air-oil lubrication system independent from the test bearing lubrication system. The hard-mounted rotor is coupled to a 20 krpm, 100 kW AC motor and its critical speed is 32,000 rpm (i.e. well above the test speed range < 15krpm).

A set of six pitch stabilizers provides a low radial stiffness while preventing rotation of the bearing respect to the rotor spin axis. Two hydraulic exciters provide the dynamic excitation in two orthogonal directions. The input excitation signal consists of a multi-tone excitation including 12 frequencies between 20 and 250 Hz. A hydraulic pull cylinder is used to apply the static load to the bearing. The loader is connected to the housing via a soft spring (~2000 lb/in) to isolate the loader mechanism from the test bearing. The lubricant, ISO VG 46, is fed to the bearing center plenum through two inlet ports in the bearing housing, and exits the bearing axially flowing to the oil sumps located at each end of the test bearing. Buffer seals at each end of the test bearing prevent the test oil from flowing into the slave bearing supports.

Figure 14 shows the 4-pad and 5-pad, 0.4 L/D, 110 mm bearings and includes all the pertinent dimensions and geometrical features.

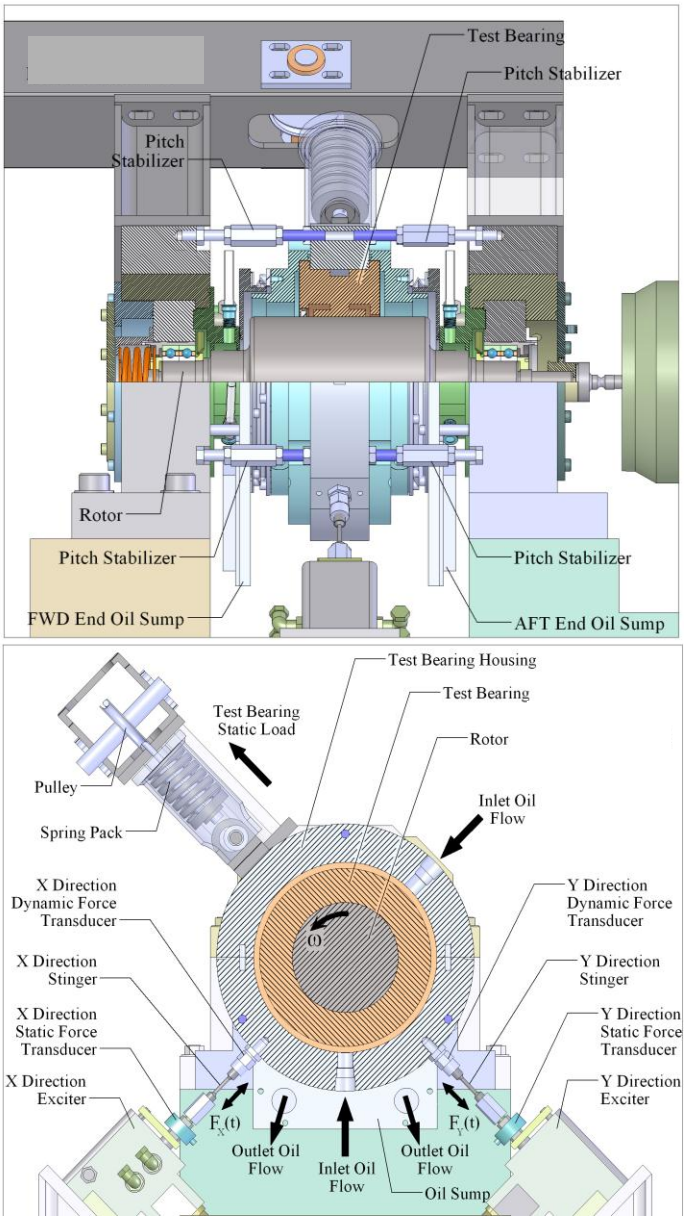

Figure 13. GE-GRC bearing test rig side and front cut views. (Delgado et al).

Bearing force coefficients

The identification of the force coefficient follows the procedure introduced by Childs and Rouvas and also implemented in the TAMU-TL tests (Eq. 2-7).

The test results are presented in terms of the stiffness-dynamic functions ($\mathbf{H}_{ij}$) as in the previous sections. The results include a single unit load (300 kPa), three test rotor speeds (7500, 10000, 15000 RPM), and display uncertainty bars that are +/- 2σ.. The 5-pad bearing tests included 0.5 and 0.6 offset, LOP and LBP configurations, while the 4-pad bearings were only tested with LBP configuration.

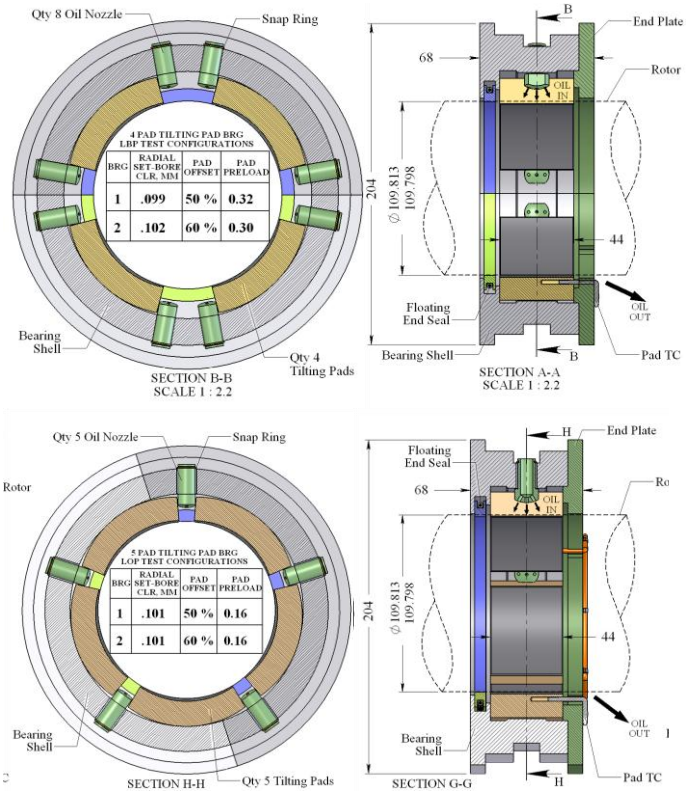

Figure 14. 4-pad and 5-pad rocker pivot bearing geometry details. (Delgado et al).

5-pad bearing

Figures 15a and 15b illustrate Re($\boldsymbol{H}_{ij}$) and Im($\boldsymbol{H}_{ij}$) for the LOP configuration for both pivot offsets (0.5, 0.6), respectively. For the 0.5 offset, Re($\boldsymbol{H}_{ij}$) show weak frequency dependence (increasing or decreasing trends) that can be captured with a mass term (i.e. using [*K*][*M*] model). Re($\boldsymbol{H}_{ij}$) showing an increasing trend with frequency are also reported by Dmochowski and by Harris and Childs for the case of lightly loaded bearings, as in the present case. The results for the 0.6 offset bearing (Fig.15a) indicate that the real part of the direct impedance is independent of the excitation frequency, which is also reported by White and Chan. For both cases (0.5 and 0.6 offset), the direct coefficients in the loaded direction (K_{yy}) are larger (25-15%) that those identified in the orthogonal unloaded direction (K_{xx}), as expected considering the level of orthotropy associated to the LOP configuration (Childs and Harris). Tables 3 and 4 present the direct force coefficients at three speeds for the 5-pad LOP and LBP configurations, respectively.

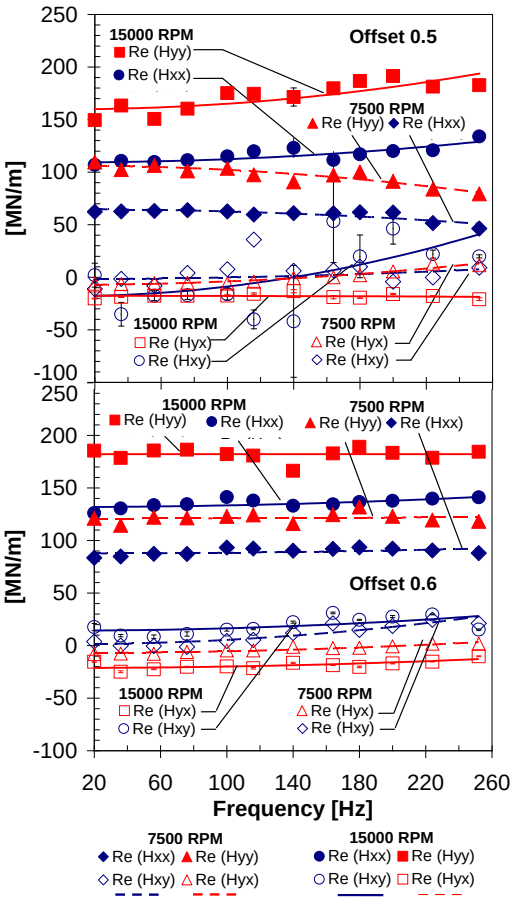

Figure 15a. Real dynamic stiffness for 5-pad, 0.5 and 0.6 offset, LOP, 300kPa bearing configuration(Delgado et al).

Figures 16a and 16b also show Re($\boldsymbol{H}_{ij}$) and Im($\boldsymbol{H}_{ij}$) for the LBP configuration. Similar to the LOP results, there is a weak to null frequency dependence of the dynamic stiffness functions. For the LBP case, the direct force coefficients in both directions are similar, which is consistent with isotropy associated to this symmetric bearing loading configuration. Comparison of the test results for the two bearings loading configurations (LOP, LBP) show that the bearing direct stiffness coefficients are similar for the loaded direction.

A common feature for all the5-pad test configurations is the frequency independence of Im($\boldsymbol{H}_{ij}$) . The results consistently show that this function is linear with frequency, and thus it can be characterized with a frequency independent damping coefficient (C_{ii}). This trend is consistent with the results reported herein from TAMU-TL tests.

Table 3. Identified force coefficients for 5-pad bearing, 0.5 and 0.6 offset LOP configurations (Delgado et al).

LOP-300kPa-0.6 offset						
Force coefficients (+/-)						
Speed (RPM)	Kxx (MN/m)	Kyy (MN/m)	Mxx (kg)	Myy (kg)	Cxx (kN.s/m)	Cyy (kN.s/m)
7500	84	117	-	-	103	129
10000	101	134	-	-	104	127
15000	129	178	-	-	101	124
Uncertainty (+/-)						
Speed (RPM)	Kxx (MN/m)	Kyy (MN/m)	Mxx (kg)	Myy (kg)	Cxx (kN.s/m)	Cyy (kN.s/m)
7500	2.347	3.05	-	-	4.221	6.746
10000	2.031	3.794	-	-	5.335	5.426
15000	2.549	4.88	-	-	4.901	7.238
LOP-300kPa-0.5 offset						
Force coefficients (+/-)						
Speed (RPM)	Kxx (MN/m)	Kyy (MN/m)	Mxx (kg)	Myy (kg)	Cxx (kN.s/m)	Cyy (kN.s/m)
7500	61	102	5.4	10.1	103	116
10000	71	112	-3.2	1.9	107	114
15000	106	157	-7.6	-13.2	127	148
Uncertainty (+/-)						
	Kxx (MN/m)	Kyy (MN/m)	Mxx (kg)	Myy (kg)	Cxx (kN.s/m)	Cyy (kN.s/m)
7500	2.2	9.0	2.6	10.6	2.2	11.5
10000	0.7	5.8	0.9	6.8	3.9	9.7
15000	3.2	19.3	3.8	22.6	5.4	28.1

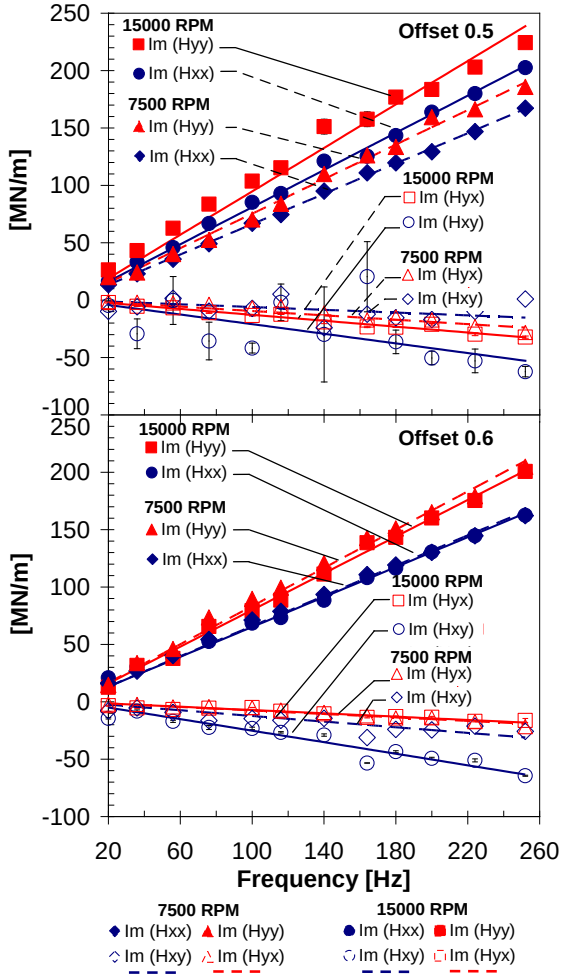

Figure 15b. Imaginary dynamic stiffness for 5-pad, 0.5 and 0.6 offset, LOP, 300kPa configuration (Delgado et al.)

Table 4. Identified force coefficients for 5-pad bearing, 0.5 and 0.6 offset LBP configurations.

LBP-300kPa-0.6 offset						
Force coefficients (+/-)						
Speed (RPM)	Kxx (MN/m)	Kyy (MN/m)	Mxx (kg)	Myy (kg)	Cxx (kN.s/m)	Cyy (kN.s/m)
7500	105	117	-4.5	-3.2	127	133
10000	122	131	-9.4	-8.8	125	131
15000	155	165	-7.3	-6.3	126	131
Uncertainty (+/-)						
Speed (RPM)	Kxx (MN/m)	Kyy (MN/m)	Mxx (kg)	Myy (kg)	Cxx (kN.s/m)	Cyy (kN.s/m)
7500	2.7	1.0	3.2	1.2	5.1	7.4
10000	2.5	1.9	2.9	2.3	7.1	6.0
15000	2.0	2.5	2.4	2.9	3.9	5.8
LBP-300kPa-0.5 offset						
Force coefficients (+/-)						
Speed (RPM)	Kxx (MN/m)	Kyy (MN/m)	Mxx (kg)	Myy (kg)	Cxx (kN.s/m)	Cyy (kN.s/m)
7500	86	114	5.1	5.5	116	124
10000	113	125	-1.2	-4.4	117	121
15000	174	173	-9.4	-15.9	137	152
Uncertainty (+/-)						
	Kxx (MN/m)	Kyy (MN/m)	Mxx (kg)	Myy (kg)	Cxx (kN.s/m)	Cyy (kN.s/m)
7500	1.8	4.3	2.1	5.0	2.2	8.1
10000	2.0	4.0	2.3	4.7	2.7	4.8
15000	3.2	6.0	3.7	7.0	7.5	8.2

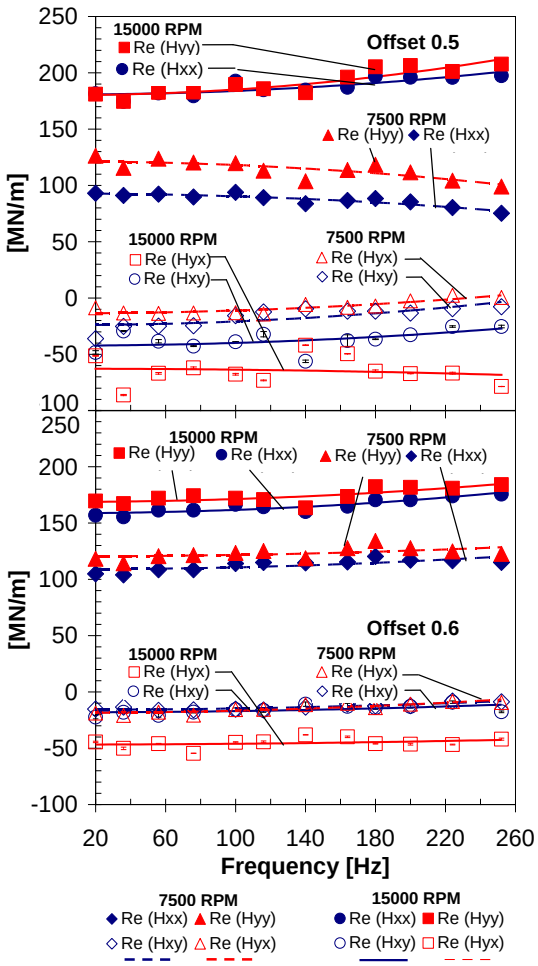

Figure 16a. Real dynamic-stiffness for 5-pad, 0.5 and 0.6 offset, LBP, 300kPa bearing configuration.

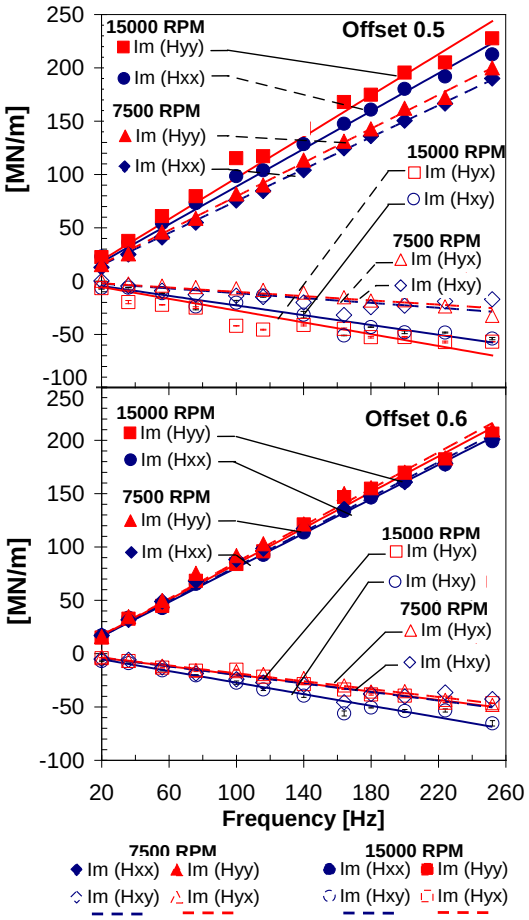

Figure 16b. Imaginary dynamic stiffness for 5-pad, 0.5 and 0.6 offset, LBP, 300kPa configuration

4-pad bearing

Figures 17a and 17b depict Re($\boldsymbol{H_{ij}}$) and Im($\boldsymbol{H_{ij}}$) associated to the 4-pad bearing, LBP configuration. Once more, Re(H_{ii}) display very small dependency on the excitation frequency, and Im(H_{ii}) can be represented with a constant damping coefficient. Table 5 lists the identified direct force coefficients for the 4-pad bearing. The identified direct force coefficients are similar to those identified from the 5-pad LBP bearing for the 0.6 pivot offset, while for the 0.5 pivot offset case, the 5-pad bearing shows consistently larger (~20 %) force coefficients for all the test speeds.

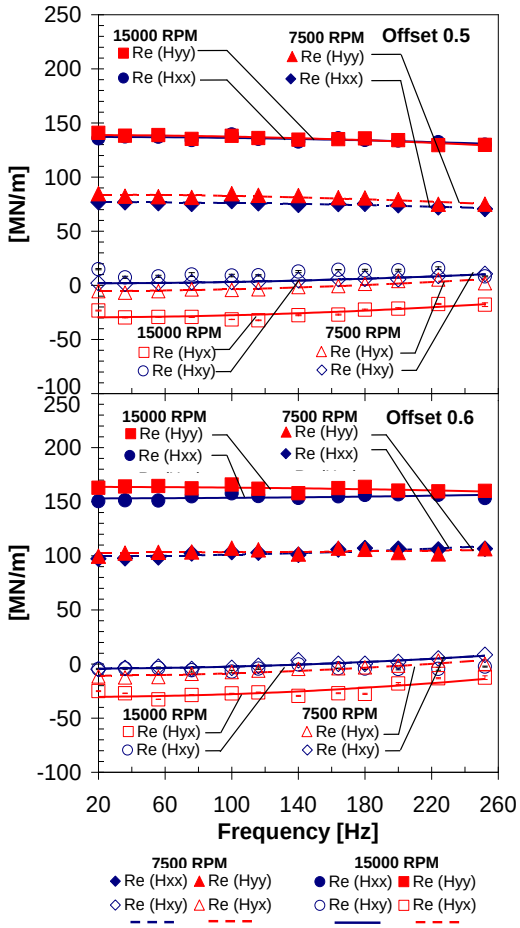

Figure 17a. Real dynamic stiffness for 4pads, 0.5, 0.6 offset, 300kPa, LBP configuration. (Delgado et al)

Table 5. Identified force coefficients for 4-pad bearing, 0.5 and 0.6 offset LOP configurations (Delgado et al).

300kPa-0.6 offset						
Force coefficients (+/-)						
Speed (RPM)	Kxx (MN/m)	Kyy (MN/m)	Mxx (kg)	Myy (kg)	Cxx (kN.s/m)	Cyy (kN.s/m)
7500	96	99	-3.6	-0.9	92	97
10000	111	119	-3.3	-2.4	85	91
15000	149	160	-1.3	1.7	75	77
Uncertainty (+/-)						
Speed (RPM)	Kxx (MN/m)	Kyy (MN/m)	Mxx (kg)	Myy (kg)	Cxx (kN.s/m)	Cyy (kN.s/m)
7500	1.2	1.4	1.8	1.4	2.1	4.0
10000	1.4	1.3	1.7	1.7	1.9	5.4
15000	1.2	2.6	1.9	1.4	3.0	4.1
300kPa-0.5 offset						
Force coefficients (+/-)						
Speed (RPM)	Kxx (MN/m)	Kyy (MN/m)	Mxx (kg)	Myy (kg)	Cxx (kN.s/m)	Cyy (kN.s/m)
7500	73.1	80.2	2.3	3.5	89.0	97.6
10000	92.5	94.4	1.0	-0.1	83.4	89.7
15000	133.2	135.0	2.5	3.8	74.6	76.8
Uncertainty (+/-)						
Speed (RPM)	Kxx (MN/m)	Kyy (MN/m)	Mxx (kg)	Myy (kg)	Cxx (kN.s/m)	Cyy (kN.s/m)
7500	0.7	0.4	0.8	0.5	3.2	4.5
10000	1.3	1.3	1.5	1.5	2.6	6.2
15000	1.2	2.2	1.4	2.6	3.7	3.4

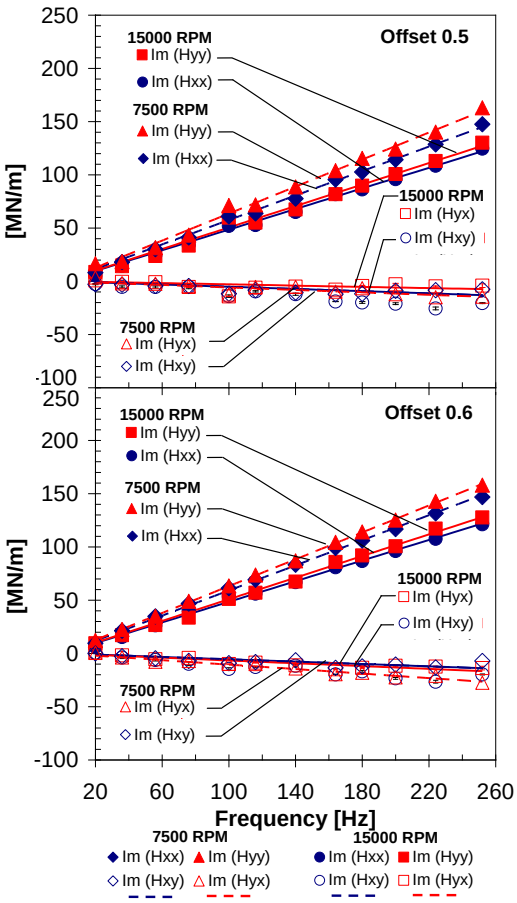

Figure 17b. Imaginary dynamic stiffness for 4pads, 0.5, 0.6 offset, 300kPa, LBP configuration (Delgado et al)

SUMMARY DISCUSSIONS AND CONCLUSIONS

The results reviewed here generally show little or no frequency dependency of stiffness and damping coefficients. Two different models can be used to define the bearing's rotordynamic coefficients. If a conventional [C][K] model is chosen, the [K] coefficients will be strongly frequency dependent because the real portions of the measured dynamic-stiffness coefficients vary with excitation frequency. For the bearings tested, an [M][C][K] model works well and eliminates the frequency dependency. Both direct and cross-coupled added-mass terms were measured; however, M_{xy} and M_{yx} have the same sign and are approximately equal. Hence, their contribution to the [M] matrix would not directly impact rotor stability.

The question of frequency dependency in rotordynamic coefficients largely centers on the subsynchronous behavior of direct-damping coefficients. If C_{yy} and C_{xx} depend on Ω, the rotor precession frequency, an iterative solution is required for stability analysis to approach $\Omega = \omega_{n1}$ where ω_{n1} is the rotor's first natural frequency. Possible frequency dependency of C_{yy} and C_{xx} for $\Omega > \omega$ are irrelevant to the stability issue. The test results cited here generally show no frequency dependency in C_{yy} and C_{xx},, an outcome that is consistent with almost all prior test programs aimed at measuring subsynchronous frequency dependency.

The result of figure 12 provide an exception, but the reduced slope with increasing frequency shown here conflicts with the generally held view of analysts who advocate frequency dependency for the direct damping coefficients.

Regarding other test programs who have examined the issue, Dmochowski presented test results for a rocker-pivot-pad bearing similar to the one illustrated in figures 9-10 and observed no frequency dependency. He had better luck predicting the measured results using a Reynolds equation model that accounted for the support flexibility of the pad. Dmochowski used very similar test procedures as those developed by the TAMU-TL.

In regard to TAMU-TL predictions, there is no issue regarding using a Reynolds-equation model or a Navier-Stokes bulk-flow model. Out to running speed, both models have about the same predictions.

The test results cited here from TAMU-TL and other researchers [19-20] were all obtained using a "shake-the stator" approach after Glenicke. As noted, these procedures and test results have been used to measure strongly frequency-dependent stiffness and damping coefficients for annular gas seals with smooth rotors and hole-pattern stators. They also produce expected results for fixed-arc bearings. Hence, unless there is some as yet unidentified dynamic feature of tilting-pad bearings that invalidates the test procedures, there is every reason to believe the measurements and question the prior (and current) predictions of frequency-dependent damping coefficients.

The test results from independent sources are in near unanimity regarding the issue of frequency dependency of stiffness and damping coefficients for tilting-pad bearings. Namely, little or no dependency has been observed for the direct damping coefficients, and the observed frequency dependency in stiffness coefficients can be readily captured via a constant [M][C][K] model. From a turbomachinery design viewpoint, the experimental results confirm the approach recommended by API 684 regarding the use of synchronously reduced coefficients for stability analysis.

NOMENCLATURE

$\boldsymbol{A_{ij}}$	Fourier transforms for the measured stator acceleration. (e.g. *Aij* is the acceleration in "*j*" direction, due to an excitation force in the "*i*" direction) [L/t^2]
C_{ij}	Direct and cross-coupled damping coefficients [F.t/L]
C_b	Radial bearing clearance [L]
D	Bearing diameter [L]
$\boldsymbol{D_{ij}}$	Fourier transforms for the measured stator relative motion [L]

$\boldsymbol{F_{ij}}$	Fourier transforms for the measured stator force [F]
F_s	Static force applied by pneumatic loader [F]
f_{bx} f_{by}	Bearing reaction force component in the *x*,*y* direction respectively [F]
f_x f_y	Measured excitation force component in the *x*,*y* direction [F]
$\boldsymbol{H_{ij}}$	Direct and cross-coupled dynamic stiffnesses [F/L]
$\boldsymbol{j}$	$\sqrt{-1}$
K_{ij}	Direct and cross-coupled stiffness coefficients [F/L]
L	Pad length [L]
M_s	Mass of the stator [M]
M_{ij}	Direct and cross-coupled added-mass coefficients [M]
P	Bearing unit load (F_s/LD) [F/L^2]
R	Bearing radius [L]
$\ddot{x}_s$ $\ddot{y}_s$	Absolute acceleration of the stator in the *x*,*y* direction [L/t^2]
Δx Δy	Relative motion between the rotor and the stator in the *x*,*y* directions [L]
Ω	Excitation frequency of stator [1/t]
ω	Running speed [1/t]

FFT	Fast Fourier Transform
LBP	Load between pad
LOP	Load on pad
TP	Tilting-pad bearing
FPTP	Flexure-pivot tilting pad bearing
WFR	Whirl frequency ratio

Subscripts

x,*y*	*x* (unloaded) and *y* (loaded) directions
i,*j*	*x*,*y*

REFERENCES

Lund, J. W. 1964, "Spring and Damping Coefficients for the Tilting-Pad Journal Bearing," ASLE Transactions, **7**, pp. 342-352 [2]

Warner, R. and Soler, A., 1975 "Stability of Rotor-Bearing Systems with Generalized Support Flexibility and Damping and Aerodynamic Cross-Coupling," ASME J. of Lubrication Technology, pp. 461-471, July.

Childs, D. "Rotordynamics of Turbomachinery... Looking Back...Looking Forward," Proceedings, IFToMM 6th International Conference on Rotordynamics, pp. 25-27 September 2002, Sydney, Australia

Glienicke, J, 1966, "Experimental Investigation of Stiffness and Damping Coefficients of Turbine Bearings and Their Application to Instability Predictions," IMechE, Proceedings of the Journal Bearings for Reciprocating and Rotating Machinery, 1966-1967, **181** (3B), pp. 116-129

Stanway, R., Burrows, C., and Holmes, R., 1978, "Pseudo-random Binary Sequence Forcing in Jounal and Squeeze Film Bearings, Proceedings. ASME Annual meeting, 78-AM-2A-1

Rouvas, C. and Childs, D., 1993, "A Parameter Identification Method for the Rotordynamic Coefficients of a High Reynolds Number Hydrostatic Bearing," ASME J. of Vibration and Acoustics, **115**, pp. 264-270.

Sprowl, B. And Childs, D., "A Study of the Effects of Inlet Preswirl on the Dynamic Coefficients of a Straight-Bore Honeycomb Gas Damper Seal," *ASME J. Of Gas Turbines*, January 2007, **129** (1), pp 220-229.

Childs, D. and Wade, J., "Rotordynamic-Coefficient and Leakage Characteristics for Hole-Pattern-Stator Annular Gas Seals — Measurements versus Predictions, "*ASME Transactions, J. of Tribology*, p. 326-333, **126**, Number 2, April 2004

Weatherwax, M., and Childs, D., 2003, "The Influence of Eccentricity on the Leakage and Rotordynamic Coefficients of a High Pressure, Honeycomb, Annular Gas Seal...Measurements versus Predictions," *ASME Transactions, J. of Tribology*, **125**, pp. 422-429

Al-Jughaiman, B., 2006, "Static and Dynamic Characteristics for a Two-Axial-Groove Bearing and a Pressure-Dam Bearing, M.S. Thesis, Texas A&M University

Al-Jughaiman, B., and Childs, D., 2008, "Static and Dynamic Characteristics for Pressure-Dam Bearing," *ASME J. For Gas Turbines*, September 2008, **130** (5), pp. 052501 1-7

Rodriguez, L. and Childs, D., 2006, "Frequency Dependency of Measured and Predicted Rotordynamic Coefficients for Load-on-Pad Flexible-Pivot Tilting-Pad Bearings, "*ASME J. of Tribology*, **128** (2), pp. 388-395

Al-Ghasem, A. and Childs, D., 2006, "Rotordynamic Coefficients; Measurements versus predictions for a High Speed Flexure-Pivot Tilting- Pad Bearing (Load-Engineering for Gas Turbines and Power, **128** (4), pp. 896-906.

Carter, C. And Childs, D., 2008 “Measurements versus Predictions for the Rotordynamic Characteristics of a 5-Pad, Rocker-Pivot, Tilting-Pad Bearing in Load between Pad Configuration,” Proceedings of ASME Turbo Expo 2008, Paper GT2008-50069, June 9-13, 2008, Berlin, Germany

Childs, D. and Carter, C., 2009, “Rotordynamic characteristics of a 5 pad, rocker-pivot, tilting pad bearing in a load-on-pad configuration; comparisons to Predictions and load-between-pad results,” ASME IGTI Turbo Expo, paper # GT2009-59696, Orlando, FL, June 2009

Harris, J. and Childs, D., “Static performance characteristics and Rotordynamic Coefficients for a four-pad Ball-in-socket Tilting Pad Journal Bearing, “ *ASME J. For Gas Turbines and Power*, November 2009, **131**(6), pp 062502 1-11

Reinhardt, E., and Lund, J., 1975, “The Influence of Fluid Inertia on the Dynamic Properties of Journal Bearings,” ASME J. of Lubrication Technology, **97**, pp. 159-167

Ball, J., and Byrne, T.,1998, Tilting Pad Hydrodynamic Bearing for Rotating Machinery, Patent Number 5,795,076, Orion Corporation, Grafton, Wisconsin

Schmied J., Fedorov, A., and Grigoriev, B., "Non-Synchronous Tilting-Pad Characteristics,” accepted for presentation at the 8th IFToMM International Conference on Rotordynamics September 12-15, 2010, KIST, Seoul, Korea

Delgado, A., Vannini, G., Ertas, B., Drexel, M., and Naldi, L., 2010, "Identification of Force Coefficients in a five-pad and a four-pad Tilting-Pad Bearing for Load-on-Pad and Load-between-Pad Configurations, GT2010-23802 in Proc. of *ASME Turbo Expo 2010: Power for Land, Sea and Air*, Glasgow, Scotland.

Dmochowski, W. 2006, "Dynamic Properties of Tilting-Pad Journal Bearings: Experimental and Theoretical Investigation of Frequency Effects Due to Pivot Flexibility," in Proc. of *ASME Turbo Expo 2006: Power for Land, Sea and Air* Barcelona, Spain.

Childs, D., and Harris, J., 2009, “Static Performance Characteristics and Rotordynamic Coefficients for a Four-Pad Ball-in-Socket Tilting Pad Journal Bearing,” J. Eng. Gas Turbines Power, **131**, pp. 062502.

White M. F., and Chan S. H., 1992, “The Subsynchronous Dynamic Behavior of Tilting-Pad Journal Bearings,” J. Tribol.,**114**(1) pp.167-174.

API 684, 2005, API Standard Paragraphs Rotordynamic Tutorial: Lateral Critical Speeds, Unbalance Response, Stability, Train Torsional and Rotor Balancing (2nd Edition), Washington D.C, API Publishing Services.